Geometry, Imaging and Computing
Volume 3, Number 1–2, 31–56, 2016

Dynamic unified surface Ricci flow

Wei Chen, Min Zhang,
Na Lei*, and David Xianfeng Gu

Surface parameterization plays a fundamental role in geometric modeling and processing. Surface Ricci flow deforms the Riemannian metric proportional to the curvature, such that the curvature evolves according to a diffusion-reaction process, and converges to the target curvature. Surface Ricci flow is a powerful tool to design Riemannian metrics from user-prescribed curvatures. In discrete setting, there are several schemes, which can be unified to a coherent framework.

Conventional discrete surface Ricci flow method is vulnerable to mesh quality. For a given target curvature and a low quality mesh, the method may encounter degeneracy. In general, it is difficult to analyze the existence of the solution to the conventional unified Ricci flow. This greatly prevents the unified Ricci flow from large-scale real applications.

In the current work, in order to conquer this problem, we propose the dynamic unified Ricci flow method. The novel method updates the triangulation during the flow, such that the triangulation is always power Delaunay. In theory, dynamic Ricci flow guarantees the existence of solutions to the flow with target curvatures satisfying Gauss-Bonnet condition; in practice, the dynamic Ricci flow is much more robust than conventional method. Our experimental results demonstrate the efficiency, efficacy and robustness of the dynamic Ricci flow method.

1. Introduction

Hamilton introduced Ricci flow for the purpose of proving Poincaré conjecture and studying 3-manifold topology. Ricci flow deforms the Riemannian metric of a manifold, such that the curvature evolves according to a diffusion-reaction process, and eventually becomes the metric inducing the target Gaussian curvature. Recently, surface Ricci flow has found many applications in a broad range of fields in both engineering and medicine. To

*Corresponding author.

name but a few, parameterization in graphics [24], deformable surface registration in vision [43], manifold spline construction in geometric modeling [16] and cancer detection in medical imaging [42]. The survey [41] cover more real applications.

1.1. Classical surface Ricci flow

Suppose $(S, \mathbf{g})$ is a surface with a Riemannian metric. One can choose a special local parameter, the so-called *isothermal coordinates* (x, y), such that the metric is represented as

$$\mathbf{g}(x, y) = e^{2u(x,y)}(dx^2 + dy^2).$$

Under the iso-thermal coordinates, the *Gaussian curvature* can be computed in a very succinct form,

$$K(x, y) = -\Delta_{\mathbf{g}} u = -\frac{1}{e^{2u(x,y)}} \left(\frac{\partial^2}{\partial x^2} + \frac{\partial^2}{\partial y^2} \right) u(x, y).$$

The *Gauss-Bonnet theorem* claims that the total Gaussian curvature is a topological invariant,

$$\int_S K dA_{\mathbf{g}} + \int_{\partial S} k_{\mathbf{g}} ds = 2\pi\chi(S),$$

where $k_{\mathbf{g}}$ is the geodesic curvature of the boundary points, $\chi(S)$ is the Euler characteristics of S. Suppose $\mathbf{g}$ and $\bar{\mathbf{g}}$ are two Riemannian metrics of a topological surface S, we say that they are *conformal equivalent* to each other, if there exists a function $u : S \to \mathbb{R}$, such that

$$\bar{\mathbf{g}} = e^{2u}\mathbf{g}.$$

The Gaussian curvatures induced by them are related by the Yamabe equation,

$$\bar{K} = e^{-2u} \left(K - \Delta_{\mathbf{g}} u \right).$$

Ricci flow deforms the Riemannian metric conformally, namely, $\mathbf{g}(t) = e^{2u(t)}\mathbf{g}(0)$, where $u(t) : S \to \mathbb{R}$ is the conformal factor. The normalized Ricci flow can be written as

$$\frac{du(t)}{dt} = \frac{2\pi\chi(S)}{A(0)} - K(t). \tag{1}$$

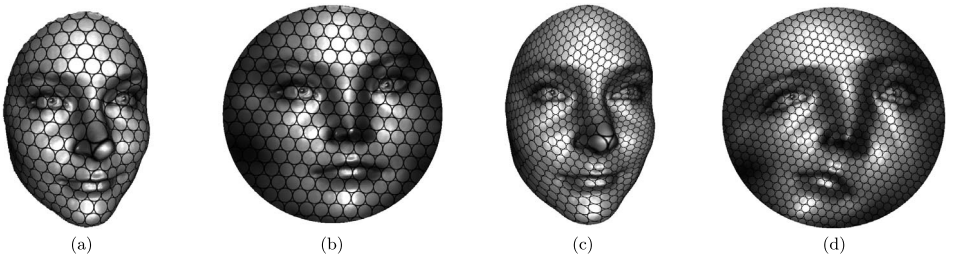

Figure 1: Conformal mapping preserves infinitesimal circles, the facial surface (a) is conformally mapped to the disk (b). General diffeomorphism maps infinitesimal ellipses to infinitesimal circles, from frame (c) to frame (d).

where $A(0)$ is the initial surface area. Hamilton [22] and chow [8] proved the convergence of surface Ricci flow. In practice, one can prescribe a target curvature $\bar{K}$, and use Ricci flow to find the unique Riemannian metric $\bar{\mathbf{g}}$ inducing $\bar{K}$,

$$\frac{du(t)}{dt} = \bar{K} - K(t).$$

Furthermore, surface Ricci flow is the negative gradient flow of the Ricci energy. Ricci energy can be minimized by convex optimization efficiently. Hence, Ricci flow has become a powerful tool for designing Riemannian metrics using prescribed curvatures, which has great potential for many applications in engineering fields.

1.2. Discrete surface Ricci flow

Conformal metric deformation transforms infinitesimal circles to infinitesimal circles as shown in Fig. 1. Intuitively, one approximates the surface by a triangulated polyhedron (a triangle mesh), covers each vertex by a disk of finite size (a cone), and deforms the disk radii preserving the combinatorial structure of the triangulation and the intersection angles among the circles. This deformation simulates the smooth conformal mapping with very high fidelity. Rodin and Sullivan [33] proved that if the triangulation of a simply connected planar domain is subdivided infinite times, the induced discrete conformal mappings converge to the smooth Riemann mapping. The discrete version of surface Ricci flow was introduced by Chow and Luo in [9] in 2003. It is based on the circle packing method.

For the purpose of computation, smooth surface Ricci flow theory has been systematically generalized to the discrete setting. Historically, many

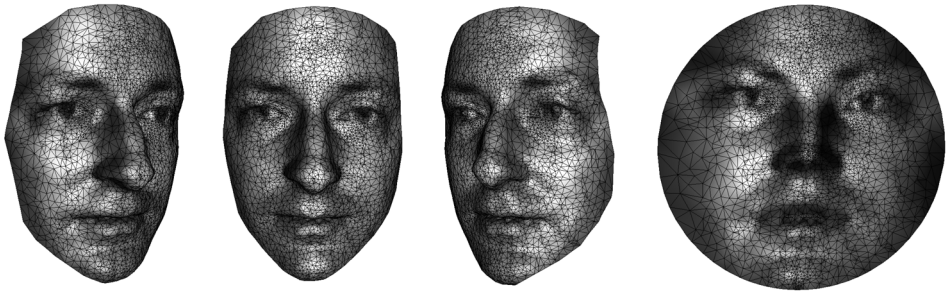

Figure 2: Robustness Test: A human facial surface is obtained by a 3D scanner, the simplification produces large number of obtuse angles. Conventional Ricci flow algorithm fails of parameterizing the mesh, whereas the dynamic Ricci flow method succeeds.

schemes of discrete surface Ricci flow have been invented. The discrete surface can be constructed by gluing Euclidean triangles isometrically along their edges. There are 6 schemes, tangential circle packing, Thurston's circle packing, inversive distance circle packing, discrete Yamabe flow, virtual radius circle packing and mixed type scheme. All these schemes can be unified to a consistent framework, namely the unified discrete surface Ricci flow [].

In practice, 3D acquisition devices produce dense point clouds, which are triangulated and simplified. The mesh simplificaiton algorithms purpose high compression rate and high fidelity, and ignore the shapes of triangles, and may produce meshes with large number of obtuse angles and skinny triangles. Such low quality meshes cause numerical instability. The conventional Ricci flow algorithm is vulnerable to triangulations with low qualities. Ricci flow deforms the edge lengths of a triangle mesh, it is possible that during the flow, the triangle inequality doesn't hold on some faces of the mesh, then the flow breaks down. In general, for inversive distance circle packing scheme or discrete Yamabe flow schemes, it is unclear how to verify whether the solution to the Ricci flow for a target curvature exists or not. The lack of theoretic foundation for the solution existence and the vulnerability to the low quality meshes prevent Ricci flow from applications in real world. Figure 2 shows one scanned human facial surface, after simplification using the method in [], the quality of the triangulation is low, and conventional Ricci flow breaks down in the computation process. In contrast, dynamic Ricci flow can handle the mesh without any difficulty, and produce the conformal mapping result as shown in the last frame.

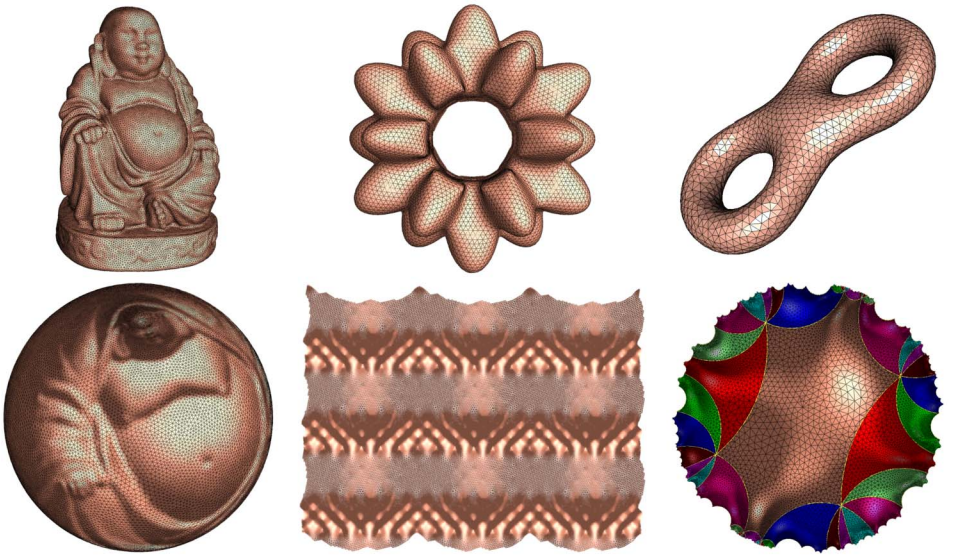

Figure 3: Uniformization for closed surfaces by Ricci flow.

1.3. Contributions

This work has following contributions:

1. This work proposes the dynamic unified surface Ricci flow framework, during the flow, the Riemannian metric evolves driven by the curvature, the connectivity is updated accordingly, such that the triangulation is always weighted Delaunay.
2. In theory, dynamic Ricci flow guarantees the existence and the uniqueness of the solutions to the flow. For any target curvature, satisfying Gauss-Bonnet condition, the discrete conformal metric exists and is essentially unique.
3. In practice, dynamic Ricci flow greatly improves the robustness to mesh quality, target curvature and topological type. This converts Ricci flow from a pure theory to a mature and reliable tool for real applications.

The paper is organized as follows: section 2 briefly reviews the most related theoretic works. Section 3 introduces the unified framework for different schemes of discrete surface Ricci flow, which covers 18 schemes in total. Section 4 gives computational algorithm. Experimental results are re-

ported in section 5, different schemes are systematically compared. The work concludes in section 6, future directions are discussed.

2. Previous works

Discrete surface Ricci flow The theoretic development of discrete surface Ricci flow has a long history. Koebe pioneered the idea of spherical circle packing in the 1930s in [25]. Andreev further developed the theory in 1970s [3, 4]. Thurston generalized their results to Euclidean (or a hyperbolic) circle packing on a triangulated closed surface with prescribed intersection angles in [37] for the purpose of studying low dimensional topology. Thurston conjectured that discrete conformal mapping induced by the circle packing converges to the conventional Riemann mapping by subdividing the triangulations to infinite levels. Rodin and Sullivan [33] proved the conjecture in 1980s. Chow and Luo [9] bridged circle packing and surface Ricci flow in 2000s. The uniqueness (rigidity) of the solution to Ricci flow based on Thurston's circle packing was proved by He Marden-Rodin [31], Colin de Verdiére [10], He [23], Thurston [37], Chow-Luo [9] and Stephenson [36].

Thurston's circle packing scheme was generalized to inversive distance circle packing by Bowers-Stephenson [7, 36]. The local rigidity and global rigidity of inversive distance circle packing were proved by Guo [20] and Luo [28] respectively.

Discrete Yamabe flow was introduced by Luo in [27]. Springborn, Schröder and Pinkall discovered the explicit formula of the energy function [35]. Glickenstein [11, 12] generalized the discrete Yamabe flow to 3-dimensional piecewise flat manifolds. Bobenko-Pinkall-Springborn introduced a geometric interpretation to Euclidean and hyperbolic Yamabe flow using the volume of generalized hyperbolic tetrahedron in [5]. Discrete Yamabe flow on hyperbolic surfaces with boundary has been studied by Guo in [19]. The existence of the solution to Yamabe flow with topological surgeries has been proved recently in [17] and [15].

Glickenstein [13] and Zhang [44] unified all the existing schemes in a coherent theoretic framework, and introduced novel schemes, such as virtual radius circle packing [41, 44] and mixed type circle packing [41, 14, 44].

Variational principle Colin de Verdiére [10] first discovered the variational approach to circle packing. Since then, many works on variational principles on circle packing or circle pattern have appeared. For example, see Brägger [39], Rivin [32], Leibon [26], Chow-Luo [9], Bobenko-Springborn [6], Guo-Luo [21], and Springborn [34]. Variational principles for polyhedral surfaces

were studied systematically in Luo [29]. Many energy functions are derived from the cosine law and its derivative [30].

Discrete uniformization Recently, the existence of the solutions to dynamic discrete Yamabe flow has been proved by Gu et al. for Euclidean and hyperbolic background geometries in [17] and [15] respectively. The theoretic results have been applied to establish the uniformization theorem for polyhedral surfaces.

3. Theoretic background

This section systematically introduces the framework for dynamic unified discrete surface Ricci flow. The theory is based on variational principle on discrete surfaces utilizing the derivative cosine law [30]. The fundamental concepts and basic schemes can be found in [29] and the chapter 4 in [41].

3.1. Fundamental concepts

In practice, smooth surfaces are usually approximated by *discrete surfaces*. Discrete surfaces are represented as two dimensional simplicial complexes which are manifolds.

Definition 1 (Triangular Mesh)**.** Suppose Σ is a two dimensional simplicial complex; furthermore, it is also a manifold. Namely, for each point p of Σ, there exists a neighborhood of p, $U(p)$, which is homeomorphic to the whole plane or the upper half plane. Then Σ is called a triangular mesh.

If $U(p)$ is homeomorphic to the whole plane, then p is called an interior point; if $U(p)$ is homeomorphic to the upper half plane, then p is called a boundary point.

The fundamental concepts from smooth differential geometry, such as Riemannian metric, curvature and conformal structure, are generalized to the simplicial complex, respectively.

In the following discussion, we use $\Sigma = (V, E, F)$ to denote the mesh with vertex set V, edge set E and face set F. A discrete surface is with Euclidean background geometry if it is constructed by isometrically gluing triangles in $\mathbb{E}^2$.

Definition 2 (Discrete Riemannian Metric)**.** A discrete metric on a triangular mesh is a function defined on the edges, $l : E \to \mathbb{R}^+$, which satisfies the

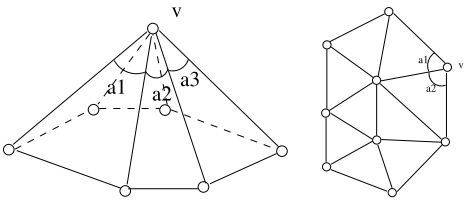

Figure 4: Discrete curvatures of an interior vertex and a boundary vertex.

triangle inequality: on each face $[v_i, v_j, v_k]$, l_i, l_j, l_k are the lengths of edges against v_i, v_j, v_k respectively,

$$l_i + l_j > l_k,\ l_j + l_k > l_i,\ l_k + l_i > l_j.$$

A triangular mesh with a discrete Riemannian metric is called a discrete metric surface.

The discrete Gaussian curvature is defined as angle deficit, as shown in Fig. 4.

Definition 3 (Discrete Gauss Curvature)**.** The discrete Gauss curvature function on a mesh is defined on vertices, $K : V \to \mathbb{R}$,

$$K(v) = \begin{cases} 2\pi - \sum_{jk} \theta_i^{jk}, & v \notin \partial M \\ \pi - \sum_{jk} \theta_i^{jk}, & v \in \partial M \end{cases}, \tag{2}$$

where θ_i^{jk}'s are corner angle at v_i in the face $[v_i, v_j, v_k]$, and ∂M represents the boundary of the mesh.

The discrete Gaussian curvature are determined bu tje discrete Riemannian metric via cosine law,

$$l_i^2 = l_j^2 + l_k^2 - 2 l_j l_k \cos\theta_i. \tag{3}$$

The Gauss-Bonnet theorem still holds in the discrete case.

Theorem 4 (Discrete Gauss-Bonnet Theorem)**.** *Suppose Σ is a triangular mesh with Euclidean background metric. The total curvature is a topological invariant,*

$$\sum_{v \notin \partial\Sigma} K(v) + \sum_{v \in \partial\Sigma} K(v) = 2\pi\chi(\Sigma), \tag{4}$$

where χ is the Euler characteristic number, and K is the Gauss curvature.

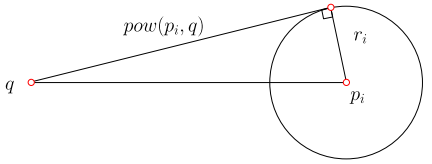

Figure 5: Power distance.

3.2. Power Delaunay triangulation

Definition 5 (Power Distance)**.** Suppose $\mathbf{p}$ and $\mathbf{q}$ are two points in $\mathbb{R}^2$, $\mathbf{p}$ is associated with a power weight h, then the power distance from $\mathbf{q}$ to $(\mathbf{p}, h)$ is defined as

$$power(\mathbf{q}, \mathbf{p}) := |\mathbf{p} - \mathbf{q}|^2 + h. \tag{5}$$

Power Voronoi diagram and power Delaunay triangulation are direct generalizations of Voronoi diagram and Delaunay triangulation. Figure 5 shows a common case, where the point $\mathbf{p}$ is associated with a circle with radius r. The power weight h equals to $-r^2$. From point $\mathbf{q}$ draw a tangent line to the circle $(\mathbf{p}, r)$, the power equals to the square of the distance from $\mathbf{q}$ to the tangent point.

Definition 6 (Power Voronoi Diagram)**.** Given a set of discrete points with power weights $P = \{(\mathbf{p}_1, h_1), (\mathbf{p}_2, h_2), \cdots, (\mathbf{p}_k, h_k)\}$, the power Voronoi diagram of P is a polygonal cell decomposition

$$\mathbb{R}^2 = \bigcup_{i=1}^{k} W_i, \quad W_i = \{\mathbf{q} \in \mathbb{R}^2 | pow(\mathbf{p}_i, \mathbf{q}) \leq pow(\mathbf{p}_j, \mathbf{q}), \forall 1 \leq j \leq k\}.$$

Definition 7 (Power Delaunay Triangulation)**.** Given a set of discrete points with power weights $P = \{(\mathbf{p}_1, h_1), (\mathbf{p}_2, h_2), \cdots, (\mathbf{p}_k, h_k)\}$, the power Delaunay triangulation is the dual to the power Voronoi diagram: if $W_i \cap W_j \neq \emptyset$ in the power Voronoi diagram, then there is an edge connecting $\mathbf{p}_i$ and $\mathbf{p}_j$ in the power Delaunay triangulation.

Figure 6 shows the power Voronoi Diagram and the dual power Delaunay triangulation.

Definition 8 (Power Center)**.** Given three weighted points $(\mathbf{p}_i, h_i)$, $(\mathbf{p}_j, h_j)$ and $(\mathbf{p}_k, h_k)$, the power center o is the unique point with equal power to

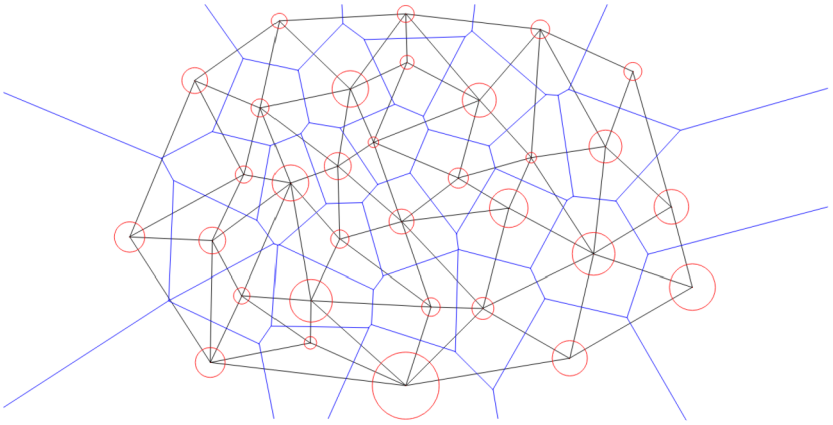

Figure 6: Power Delaunay triangulation and power Voronoi diagram.

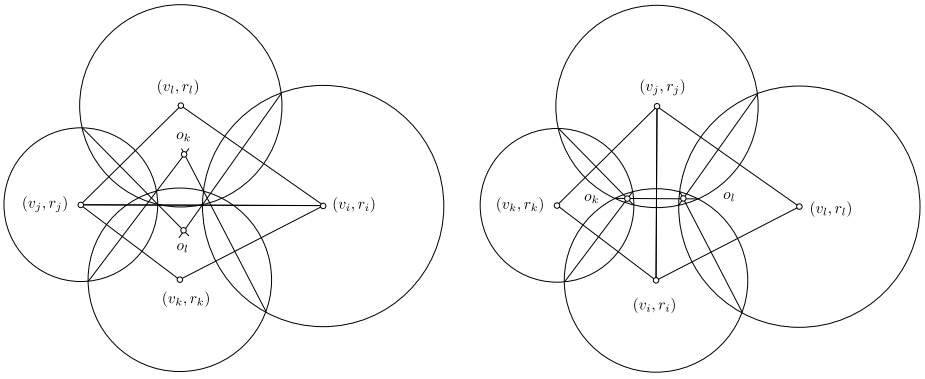

(a) non-Power Delaunay (b) power Delaunay

Figure 7: Construct power Delaunay triangulation by edge flipping.

these three points.

$$pow(\mathbf{p}_i, o) = pow(\mathbf{p}_j, o) = pow(\mathbf{p}_k, o)$$

As shown in Figure 7, if two circles $(\mathbf{p}_i, r_i)$ and $(\mathbf{p}_j, r_j)$ intersects, then the equi-power line is the common chord of the two circles. The intersection between two equi-power lines is the power center of the triangle. If all three circles are disjoint, then there is a unique circle $(\mathbf{o}, r)$ orthogonal to all of them, the center $\mathbf{o}$ is the power center, r^2 is the power from the center to every vertex.

In fact, as shown in Figure 6, the vertices in power Voronoi diagram are the power centers of the triangles in power Delaunay triangulation. Each edge $[v_i, v_j]$ in Delaunay triangulation is adjacent to two triangles $[v_i, v_j, v_k]$ and $[v_j, v_i, v_l]$, the corresponding power centers are $\mathbf{o}_k$ and $\mathbf{o}_l$ respectively. The oriented edge $[\mathbf{o}_l, \mathbf{o}_k]$ is the edge in the Voronoi diagram, dual to the oriented edge $[v_i, v_j]$ in the triangulation. The triangulation is power Delaunay, if and only if

$$pow(\mathbf{o}_k, \mathbf{p}_k) \leq pow(\mathbf{o}_k, \mathbf{p}_l), \qquad pow(\mathbf{o}_l, \mathbf{p}_l) \leq pow(\mathbf{o}_l, \mathbf{p}_k).$$

Equivalently, the triangulation is power Delaunay, if and only if for each interior edge $[v_i, v_j]$,

$$(v_j - v_i) \times (\mathbf{o}_k - \mathbf{o}_l) > 0.$$

One can obtain the power Delaunay triangulation by edge flipping operations as shown in Figure 7. One can iteratively check all the interior edges; if one edge is not power Delaunay then flip it, until all edges are power Delaunay. This simple algorithm can produce power Delaunay triangulation effectively.

3.3. Unified circle packing metrics

Definition 9 (Circle Packing Metric)**.** Suppose $\Sigma = (V, E, F)$ is a triangle mesh with spherical, Euclidean or hyperbolic background geometry. Each vertex v_i is associated with a circle with radius γ_i. The circle radius function is denoted as $\gamma : V \to \mathbb{R}_{>0}$; a function defined on the vertices $\epsilon : V \to \{+1, 0, -1\}$ is called the *scheme coefficient*; a function defined on edges $\eta : E \to \mathbb{R}$ is called the *discrete conformal structure coefficient*. A circle packing metric is a 4-tuple $(\Sigma, \gamma, \eta, \epsilon)$, the edge length is determined by the 4-tuple and the background geometry.

In the smooth case, changing a Riemannian metric by a scalar function, $\mathbf{g} \to e^{2u}\mathbf{g}$, is called a conformal metric deformation. The discrete analogy to this is as follows.

Definition 10 (Discrete Conformal Equivalence)**.** Two circle packing metrics $(\Sigma_k, \gamma_k, \eta_k, \epsilon_k)$, $k = 1, 2$, are conformally equivalent if $\Sigma_1 = \Sigma_2$, $\eta_1 = \eta_2$, $\epsilon_1 = \epsilon_2$. (γ_1 may not equals to γ_2.)

The discrete analogy to the concept of conformal factor in the smooth case is

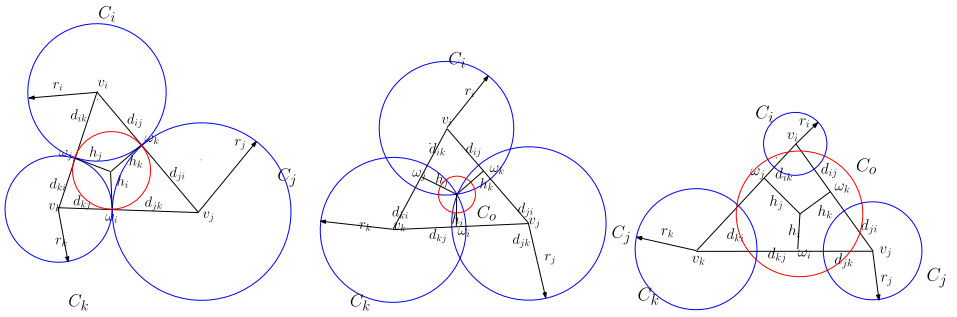

(a) tangential CP $\eta = 1, \epsilon = 1$ (b) Thurston's CP $0 \leq \eta \leq 1, \epsilon = 1$ (c) Inversive distance CP $\eta \geq 1, \epsilon = 1$

Figure 8: Tangential circle packing, Thurston's circle packing and inversive distance circle packing schemes, and the geometric interpretations to their Ricci energies.

Definition 11 (Discrete Conformal Factor)**.** Discrete conformal factor for a circle packing metric $(\Sigma, \gamma, \eta, \epsilon)$ is a function defined on each vertex $\mathbf{u} : V \to \mathbb{R}$,

$$u_i = \log \gamma_i \tag{6}$$

Definition 12 (Circle Packing Schemes)**.** Suppose $\Sigma = (V, E, F)$ is triangle mesh with spherical, Euclidean or hyperbolic background geometry. Given a circle packing metric $(\Sigma, \gamma, \eta, \epsilon)$, for an edge $[v_i, v_j] \in E$, its length l_{ij} is given by

$$l_{ij}^2 = 2\eta_{ij} e^{u_i + u_j} + \varepsilon_i e^{2u_i} + \varepsilon_j e^{2u_j}. \tag{7}$$

The schemes are named as follows:

Scheme	ε_i	ε_j	η_{ij}
Tangential Circle Packing	$+1$	$+1$	$+1$
Thurston's Circle Packing	$+1$	$+1$	$[0, 1]$
Inversive Distance Circle Packing	$+1$	$+1$	> 0
Yamabe Flow	0	0	> 0
Virtual Radius Circle Packing	-1	-1	> 0
Mixed type	$\{-1, 0, +1\}$	$\{-1, 0, +1\}$	> 0

Fig. 8 and Fig. 9 illustrate all the schemes with for discrete surfaces with Euclidean background geometry.

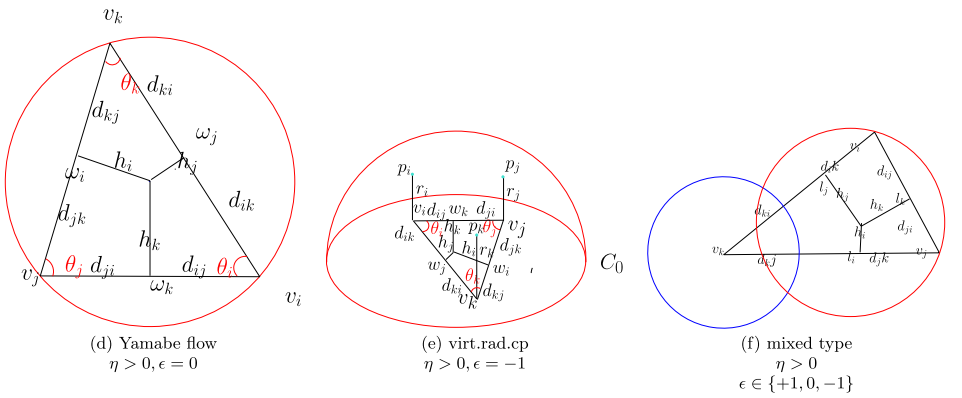

(d) Yamabe flow
$\eta > 0, \epsilon = 0$

(e) virt.rad.cp
$\eta > 0, \epsilon = -1$

(f) mixed type
$\eta > 0$
$\epsilon \in \{+1, 0, -1\}$

Figure 9: Yamabe flow, virtual radius circle packing and mixed type schemes, and the geometric interpretations to their Ricci energies.

Remark 13. From the definition, the tangential circle packing is a special case of Thurston's circle packing; Thurston's circle packing is a special case of inversive distance circle packing. In the following discussion, we unify all three types as inversive distance circle packing.

3.4. Discrete surface Ricci flow

Definition 14 (Discrete Surface Ricci Flow)**.** A discrete surface with $\mathbb{S}^2$, $\mathbb{E}^2$ or $\mathbb{H}^2$ background geometry, and a circle packing metric $(\Sigma, \gamma, \eta, \epsilon)$, the discrete surface Ricci flow is

$$\frac{du_i(t)}{dt} = \bar{K}_i - K_i(t), \tag{8}$$

where $\bar{K}_i$ is the target curvature at the vertex v_i.

The target curvature must satisfy certain constraints to ensure the existence of the solution to the flow, such as Gauss-Bonnet equation Eqn. 4, but also some additional ones described in [37], [31] and [9], for instances.

The discrete surface Ricci flow has exactly the same formula as the smooth counter part Eqn. 1. Furthermore, similar to the smooth case, discrete surface Ricci flow is also variational: the discrete Ricci flow is the negative gradient flow of the discrete Ricci energy.

Definition 15 (Discrete Ricci Energy)**.** A discrete surface with $\mathbb{S}^2$, $\mathbb{E}^2$ or $\mathbb{H}^2$ background geometry, and a circle packing metric $(\Sigma, \gamma, \eta, \epsilon)$. For a triangle

$[v_i, v_j, v_k]$ with inner angles $(\theta_i, \theta_j, \theta_k)$, the discrete Ricci energy on the face is given by

$$E_f(u_i, u_j, u_k) = \int^{(u_i,u_j,u_k)} \theta_i du_i + \theta_j du_j + \theta_k du_k. \tag{9}$$

The discrete Ricci energy for the whole mesh is defined as

$$E_\Sigma(u_1, u_2, \cdots, u_n) = \int^{(u_1,u_2,\cdots,u_n)} \sum_{i=1}^{n} (\bar{K}_i - K_i) du_i.. \tag{10}$$

From definition, we get the relation between the surface Ricci energy and the face Ricci energy

$$E_\Sigma = \sum_{i=1}^{n} (\bar{K}_i - 2\pi) u_i + \sum_{f \in F} E_f. \tag{11}$$

The Hessian matrix of the energy has intuitive geometric interpretation.

3.5. Geometric interpretation to Hessian

The interpretation in Euclidean case is due to Glickenstein [13] (Z. He [40] in the case of circle packings) and illustrated in [41]. In the current work, we build the connection to the Power Delaunay triangulation and power voronoi diagram.

We only focus on one triangle $[v_i, v_j, v_k]$, with corner angles $\theta_i, \theta_j, \theta_k$, conformal factors u_i, u_j, u_k and edge lengths l_{ij} for edge $[v_i, v_j]$, l_{jk} for $[v_j, v_k]$ and l_{ki} for $[v_k, v_i]$.

As shown in Fig. 8 and Fig. 9, the *power* of q with respect to v_i is

$$pow(v_i, q) = |v_i - q|^2 - \epsilon\gamma_i^2.$$

The *power center* o of the triangle satisifies

$$pow(v_i, o) = pow(v_j, o) = pow(v_k, o).$$

The *power circle* C centered at o with radius γ, where $\gamma = pow(v_i, o)$.

Therefore, for tangential, Thurton's and inversive distance circle packing cases, the power circle is orthogonal to three circles at the vertices C_i, C_j and C_k; for Yamabe flow case, the power circle is the circumcircle of the

triangle; for virtual radius circle packing, the power circle is the equator of the sphere, which goes through three points $\{v_i + \gamma_i^2\mathbf{n}, v_j + \gamma_j^2\mathbf{n}, v_k + \gamma_k^2\mathbf{n}\}$, where $\mathbf{n}$ is the normal to the plane.

Through the power center, we draw line perpendicular to three edges, the perpendicular feets are w_i, w_j and w_k respectively. The distance from the power center to the perpendicular feet are h_i, h_j and h_k respectively. Then it can be shown easily that

$$\frac{\partial\theta_i}{\partial u_j} = \frac{\partial\theta_j}{\partial u_i} = \frac{h_k}{l_k}, \frac{\partial\theta_j}{\partial u_k} = \frac{\partial\theta_k}{\partial u_j} = \frac{h_i}{l_i}, \frac{\partial\theta_k}{\partial u_i} = \frac{\partial\theta_i}{\partial u_k} = \frac{h_j}{l_j}, \tag{12}$$

furthermore,

$$\frac{\partial\theta_i}{\partial u_i} = -\frac{h_k}{l_k} - \frac{h_j}{l_j}, \frac{\partial\theta_j}{\partial u_j} = -\frac{h_k}{l_k} - \frac{h_i}{l_i}, \frac{\partial\theta_k}{\partial u_k} = -\frac{h_i}{l_i} - \frac{h_j}{l_j}. \tag{13}$$

These two formula induces the formula for the Hessian of the Ricci energy of the whole surface. One can treat the circle packing $(\Sigma, \gamma, \eta, \varepsilon)$ as a power triangulation, which has a dual power diagram $\bar{\Sigma}$. Each edge $e_{ij} \in \Sigma$ has a dual edge $\bar{e} \in \bar{\Sigma}$, then one define the *edge weight* as

$$w_{ij} = \frac{|\bar{e}_{ij}|}{|e_{ij}|}, \tag{14}$$

Here $|\cdot|$ represent the signed distance of an edge, if the edge e_{ij} is power Delaunay, then the weight w_{ij} is non-negative; otherwise, the weight is negative. Hence

$$\frac{\partial K_i}{\partial u_j} = \frac{\partial K_j}{\partial u_i} = w_{ij}, \tag{15}$$

and

$$\frac{\partial K_i}{\partial u_i} = -\sum_j w_{ij}. \tag{16}$$

Namely, the Hessian matrix of the Ricci energy is a discrete Laplace-Beltrami matrix.

Suppose on the edge $[v_i, v_j]$, the distance from v_i to the perpendicular foot w_k is d_{ij}, the distance from v_j to w_k is d_{ji}, then $l_{ij} = d_{ij} + d_{ji}$, and

$$\frac{\partial l_{ij}}{\partial u_i} = d_{ij}, \frac{\partial l_{ij}}{\partial u_j} = d_{ji},$$

furthermore

$$d_{ij}^2 + d_{jk}^2 + d_{ki}^2 = d_{ik}^2 + d_{kj}^2 + d_{ji}^2.$$

The existence of solution to the discrete Yambe flow has been proved in a recent work [17].

Theorem 16. *Given a topological surface S, with vertex set V, and a flat metric d with cone singularities at V, for any target curvature $\bar{K} : V \to (-\infty, 2\pi)$, satisfying Gauss-Bonnet condition, the dynamic discrete Yambe flow will converge to the flat metric $\bar{d}$ inducing $\bar{K}$. Furthermore $\bar{d}$ is unique upto a scaling.*

4. Computational algorithm

In this section, we explain the dynamic unified surface Ricci flow algorithm 1 in details.

Algorithm 1 Dynamic Unified Surface Ricci Flow

Require: The inputs include:
1. A triangular mesh Σ, embedded in $\mathbb{E}^3$;
2. The circle packing scheme, $\epsilon \in \{+1, 0, -1\}$;
3. A target curvature $\bar{K}$, $\sum \bar{K}_i = 2\pi\chi(\Sigma)$ and $\bar{K}_i \in (-\infty, 2\pi)$.
4. Step length δt

Ensure: A discrete metric conformal to the original one, which realizes the target curvature $\bar{K}$.

Initialize the circle radii γ, discrete conformal factor u and conformal structure coefficient η, obtain the initial circle packing metric $(\Sigma, \gamma, \eta, \epsilon)$
while $\max_i |\bar{K}_i - K_i| > threshold$ **do**
  Compute the circle radii γ from the conformal factor u
  Compute the edge length from γ and η
  Compute the corner angle θ_i^{jk} from the edge length using cosine law
  Compute the Power center of each face
  Update the triangulation to be power Delaunay
  Compute the vertex curvature K
  Compute the edge weight, form the Hessian matrix H
  Solve linear system $H\delta u = \bar{K} - K$
  Update conformal factor $u \leftarrow u - \delta t \times \delta u$
end while
Output the result circle packing metric

Step 1. Initial circle packing (γ, η) Depending on different schemes, the initialization of the circle packing is different. The mesh has induced Euclidean metric l_{ij}. For inversive distance circle packing, we choose

$$\gamma_i = \frac{1}{3} \min_j l_{ij},$$

this ensures all the vertex circles are separated. For Yamabe flow, we choose all γ_i to be 1. For virtual radius circle packing, we choose all γ_i's to be 1. Then γ_{ij} can be computed using the l_{ij} formula Eqn. 7.

Step 2. Circle radii γ The computation for circle radii from conformal factor uses the formula in Eqn. 6.

Step 3. Edge length l The computation of edge lengths from conformal factor u and conformal structure coefficient η uses the formulae in Eqn. 7.

Step 4. Update triangulation We compute the power center of each face using the current edge length, and perform edge swap to update the triangulation to be weighted Delaunay.

Step 5. Corner angle θ The computation from edge length l to the corner angle θ uses the cosine law formulae, Eqn. 3

Step 6. Vertex curvature K The vertex curvature is defined as angle deficit in Eqn. 2

Step 7. Hessian matrix H We compute the power center of each face, and then the edge weight using formula Eqn. 12 and form the Hessian matrix as in Eqn. 13.

Step 8. Linear system If the Σ is with $\mathbb{H}^2$ background geometry, then the Hessian matrix H is positive define; else if Σ is with $\mathbb{E}^2$ background geometry, then H is positive definite on the linear subspace $\sum_i u_i = 0$. The linear system can be solved using any sparse linear solver, such as Eigen [18].

5. Experimental results

In this section, we report our experimental results for the proposed dynamic unified discrete surface flow. We tested the robustness of the proposed algorithm to low quality meshes, extremal target curvatures, complicated topologies, and tested the convergence speed.

5.1. Experimental environment

The dynamic unified Ricci flow algorithms are implemented using generic C++ language on Windows platform. The computational time is tested on a desktop computer with 2.00GHz CPU, 3.00G RAM. The algorithm depends

on convex optimization by Newton's method. The sparse linear systems are solved using Eigen library [18].

Dynamic Ricci flow modifies the connectivity, such that the triangulations could become complicated. Conventional halfedge data structure can not support general triangulations. For example, in generalized triangulation, the two end vertices of an edge may coincide, such as a triangulation of a torus with a single vertex and three edges. Therefore, we have to use more sophisticated dynamic halfedge data-structure. The current implementation covers all schemes, and including inversive distance circle packing, Yambe flow, virtual radius circle packing and mixed type schemes, for discrete surfaces with Euclidean background geometry.

The geometric data sets are from the public databases, such as [1] and [2]. The human face surfaces were scanned from a high speed and high resolution, phase shifting scanner, as described in [38]. We thoroughly tested our algorithm on a huge amount of various models, including different sizes and topology types.

5.2. Robustness to low quality meshes

Human facial surfaces are obtained by a 3D scanning system. The initial surface has dense samples, in order to reduce the storage, the raw geometric data is simplified using various mesh simplification method. One popular method is based on Hoppy's progressive mesh, which reduce the geometric complexity by edge collapsing. This method maximizes the compression ratio, and minimizes the approximation error, but ignore the mesh quality. As shown in Fig. 2, by zooming in the figure, we can see that the simplified mesh has many skinny triangles and obtuse angles. Especially, along the boundary of the surface, there are many vertices which are adjacent to a single face. These factors makes the conventional Ricci flow method highly unstable. We have tested conventional Ricci flow algorithms based on inversive circle packing, Yambe flow, virtual radius circle packing on the data sets shown in Fig. 2, Fig. 10 and Fig. 11, none of them can handle all the data sets. In contrast, the dynamic Ricci flow with the same schemes can handle all of them, and produce accurate conformal parameterizations.

5.3. Robustness to extremal target curvatures

Given a target curvature $\bar{K}$, it is difficult to verify if the solution to the conventional Ricci flow exists or not. The theoretic uncertainty prevents the method from practical applications, which require reliability. According to

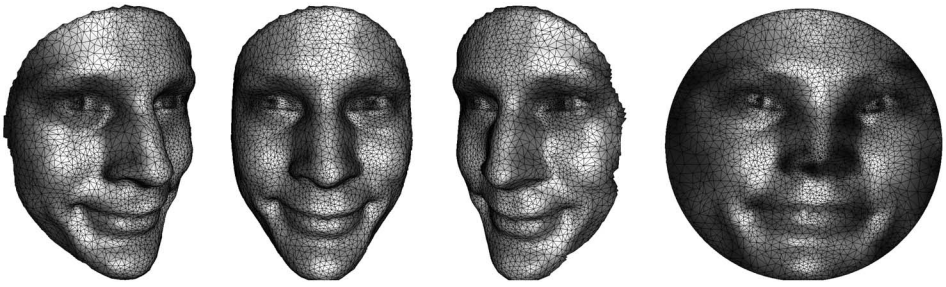

Figure 10: Robustness testing with low quality human facial surfaces.

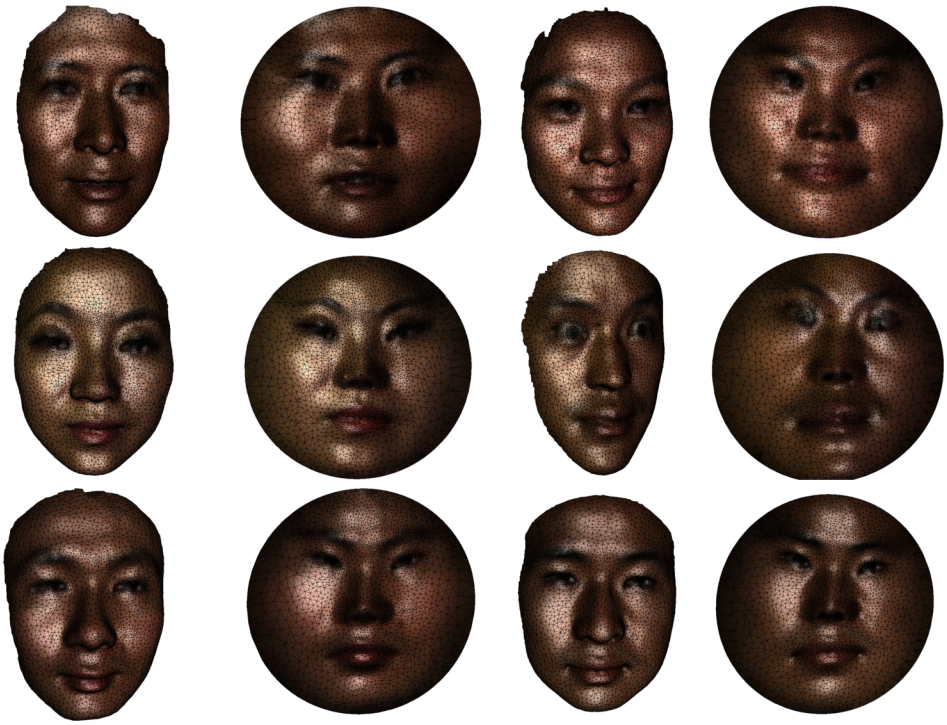

Figure 11: Robustness testing with low quality human facial surfaces.

Theorem 16, if the target curvature satisfies Gauss-Bonnet condition and is less than 2π, then the solution to the dynamic Ricci flow is guaranteed to exist. This makes dynamic Ricci flow reliable and dependable. We tested the robustness of the proposed method by setting some extremal target curvatures, which concentrate all the curvatures on a few vertices. Figure 12

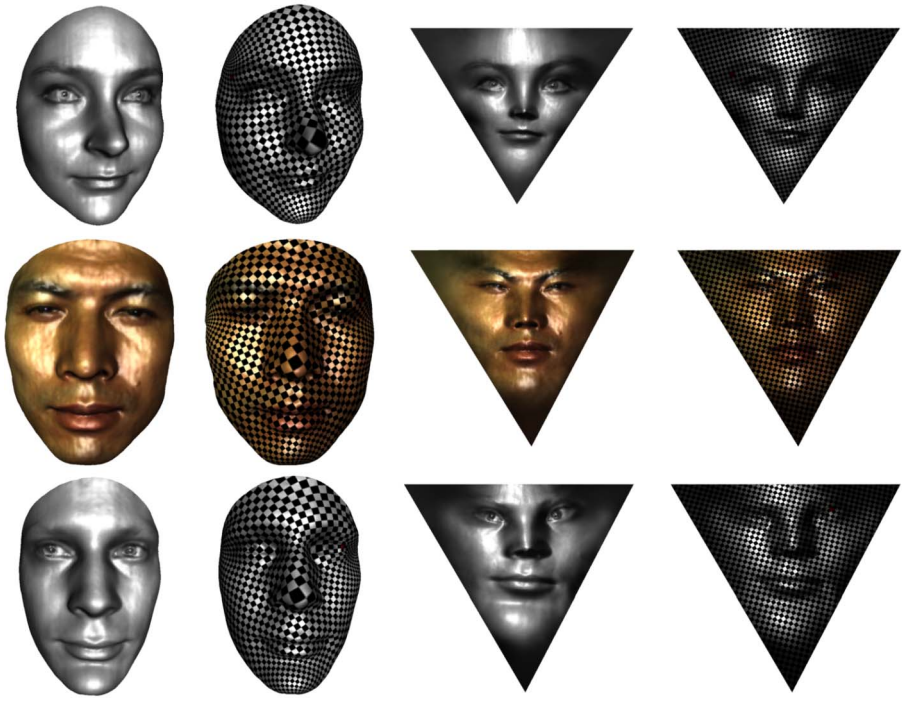

Figure 12: Robustness testing with extremal target curvatures, which concentrate the total curvature on just 3 vertices.

shows several testing results, where we set the target curvature to be zeros everywhere, except three boundary vertices. This maps the whole surface onto a planar triangle. Dynamic Ricci flow can find the solution reliably, whereas conventional Ricci flow heavily depends on the triangulation, and the behavior is unpredictable.

Furthermore, we also tested our proposed algorithm on high genus surfaces. For a genus $g > 0$ surface, we concentrate all the curvature on a single vertex v_0, $K(v_0) = (4 - 4g)\pi$, and the target curvature is zero for any other vertex. The dynamic Ricci flow can find the desired metric with many edge swapping. Conventional Ricci flow method always encounters degenerated faces during the flow.

5.4. Robustness to topological types

Dynamic Ricci flow can handle surfaces with all possible topological types. Figure 3 shows our experimental results on closed surfaces with different

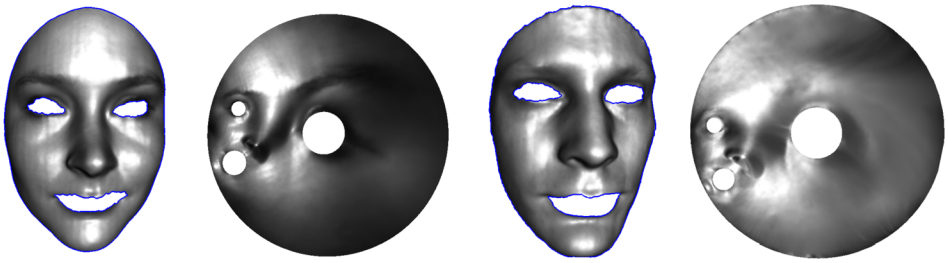

Figure 13: Robustness testing with complicated topological types.

genus. Figure 13 shows the computational results for surfaces with boundaries. Conformal parameterization for poly-annulus is highly non-linear, and challenging. With low mesh quality, conventional Ricci flow method is difficult to find the conformal mapping from the surface to the canonical planar circle domain, such that all boundaries are mapped to Euclidean circles. We tested the proposed dynamic Ricci flow algorithm for parameterizing poly-annulus, with relatively low mesh quality, the method can compute the conformal mapping straight-forwardly. This demonstrates the robustness of the method to complicated topological types.

5.5. Convergence speed and efficiency

We further tested the efficiency of our proposed dynamic Ricci flow algorithm on various models. The experimental results are summarized in Figure 14 and Table 1. The geometric complexity of the models in terms of vertex, face and edge numbers are given in the table, the running time (seconds) and the number of iterations are reported. The curvature threshold for the difference between the current curvature and the target curvature is chose to be $1e-8$. From the table, it is clear that dynamic Ricci flow converges to the desired metric after less than ten iterations. This experiment demonstrates the fast convergence speed of dynamic Ricci flow method.

6. Conclusion

This work introduces a dynamic unified Ricci flow, which updates the connectivity during flow to preserve the triangulation to be power Delaunay. The unified framework improves the flexibility of Ricci flow; the dynamic scheme makes the connectivity to adapt to the intrinsic Riemannian metric, and therefore guarantees the existence of the solutions to the Ricci flow as

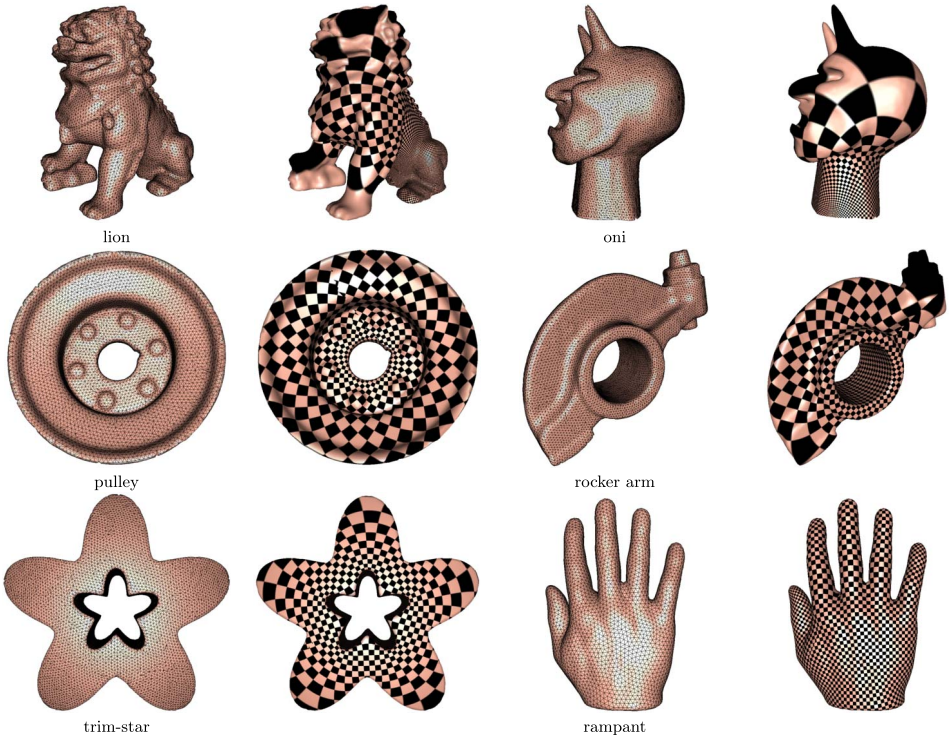

Figure 14: Convergence speed and efficiency test.

Table 1: Convergence test

mesh	V/F/E	Genus	Ricci Flow	Dynamic Ricci Flow (Sec/Iters)
lion	11489/22853/34341	0	invalid	12.068/6
Oni	12479/24855/37333	0	invalid	16.089/7
Pulley	12395/24790/37185	1	invalid	5.027/6
Rocker Arm	12442/24884/37326	1	invalid	5.037/5
Trim Star	12488/24976/37464	1	invalid	5.032/6
Bumpy Torus	12522/25044/37566	1	invalid	8.001/5
Rampant	49873/99746/149619	1	invalid	28.026/9

long as the target curvature satisfies Gauss-Bonnet condition. The dynamic Ricci flow greatly improves the robustness, and is capable of handling meshes with low qualities and complicated topologies. This makes the theoretic tool useful and reliable for practical applications in real world.

In the future, we will generalize dynamic surface Ricci flow from Eu-

clidean background geometry to hyperbolic background geometry, and explore discrete Ricci flow on high dimensional manifolds.

Acknowledgement

This project has been partially supported by NSFC 11271156, AFOSR FA9550-14-1-0193, NSF DMS-1418255, NSFC 61303078.

References

[1] The digital Michelangelo project. https://graphics.stanford.edu/projects/mich/, 1997.

[2] Repository of aim@shape project. http://shapes.aimatshape.net/, 1997.

[3] E. M. Andreev. Complex polyhedra in Lobachevsky spaces. *(Russian) Mat. Sb. (N.S.)*, 81(123):445–478, 1970.

[4] E. M. Andreev. Convex polyhedra of finite volume in Lobachevsky space. *(Russian) Mat. Sb. (N.S.)*, 83(125):256–260, 1970.

[5] A. Bobenko, U. Pinkall, and B. Springborn. Discrete conformal maps and ideal hyperbolic polyhedra. arXiv:1005.2698, 5 2010.

[6] A. I. Bobenko and B. A. Springborn. Variational principles for circle patterns and Koebe's theorem. *Trans. Amer. Math. Soc.*, 356(2):659–689, 2004.

[7] P. L. Bowers and K. Stephenson. Uniformizing dessins and Belyi maps via circle packing. *Mem. Amer. Math. Soc.*, 170(805), 2004.

[8] B. Chow. The Ricci flow on the 2-sphere. *Journal of Differential Geometry*, 33(2):325–334, 1991. MR1094458

[9] B. Chow and F. Luo. Combinatorial Ricci flows on surfaces. *Journal Differential Geometry*, 63(1):97–129, 2003.

[10] Y. C. de Verdiére. Un principe variationnel pour les empilements de cercles. *Invent. Math.*, 104:655–669, 1991.

[11] D. Glickenstein. A combinatorial Yamabe flow in three dimensions. *Topology*, 44(4):791–808, 2005.

[12] D. Glickenstein. A maximum principle for combinatorial Yamabe flow. *Topology*, 44(4):809–825, 2005.

[13] D. Glickenstein. Discrete conformal variations and scalar curvature on piecewise flat two and three dimensional manifolds. *Journal of Differential Geometry*, 87(2):201–238, 2011. MR2788656

[14] D. Glickenstein. Problems in combinatorial and numerical Ricci flow. Talk in Workshop: Perspective Of The Ricci Flow, 2 2013.

[15] X. Gu, R. Guo, F. Luo, J. Sun, and T. Wu. A discrete uniformization theorem for polyhedral surfaces ii. *arXiv:1401.4594*, 2014.

[16] X. Gu, Y. He, M. Jin, F. Luo, H. Qin, and S.-T. Yau. Manifold splines with a single extraordinary point. *Computer-Aided Design*, 40(6):676–690, 2008.

[17] X. Gu, F. Luo, J. Sun, and T. Wu. A discrete uniformization theorem for polyhedral surfaces. *arXiv:1309.4175*, 2013.

[18] G. Guennebaud, B. Jacob, et al. Eigen. http://eigen.tuxfamily.org, 2010.

[19] R. Guo. Combinatorial Yamabe flow on hyperbolic surfaces with boundary. *Communications in Contemporary Mathematics*, 13(5):827–842, 2011.

[20] R. Guo. Local rigidity of inversive distance circle packing. *Trans. Amer. Math. Soc.*, 363:4757–4776, 2011.

[21] R. Guo and F. Luo. Rigidity of polyhedral surface ii. *Geom. Topol.*, 13:1265–1312, 2009.

[22] R. Hamilton. Ricci flow on surfaces. *Mathematics and General Relativity, Contemporary Mathematics AMS, Providence, RI,*, 71:237–261, 1988.

[23] Z.-X. He and O. Schramm. On the convergence of circle packings to the Riemann map. *Invent. Math.*, 125:285–305, 1996.

[24] M. Jin, J. Kim, F. Luo, and X. Gu. Discrete surface Ricci flow. *IEEE Transactions on Visualization and Computer Graphics*, 14(5):1030–1043, 2008.

[25] P. Koebe. Kontaktprobleme der konformen abbildung. *Ber. Sächs. Akad. Wiss. Leipzig, Math. Phys. Kl.*, 88:141–164, 1936.

[26] G. Leibon. Characterizing the Delaunay decompositions of compact hyperbolic surface. *Geom. Topol.*, 6:361–391, 2002.

[27] F. Luo. Combinatorial Yamabe flow on surfaces. *Contemp. Math.*, 6(5):765–780, 2004.

[28] F. Luo. Rigidity of polyhedral surfaces, iii. *Geometry and Topology*, 15(4):2299–2319, December 2011.

[29] F. Luo. Rigidity of polyhedral surfaces. *Journal of Differential Geometry*, 96(1):241–302, 2014.

[30] F. Luo, X. Gu, and J. Dai. *Variational Principles for Discrete Surfaces*. Advanced Lectures in Mathematics. High Education Press and International Press, 2007.

[31] A. Marden and B. Rodin. *Computational methods and function theory (Valpara'iso, 1989)*, volume 1435 of *Lecture Notes in Math.*, chapter On Thurston's formulation and proof of Andreev's theorem, pages 103–116. Springer, Berlin, 1990.

[32] I. Rivin. Euclidean structures of simplicial surfaces and hyperbolic volume. *Ann. of Math.*, 139:553–580, 1994.

[33] B. Rodin and D. Sullivan. The convergence of circle packings to the Riemann mapping. *Journal of Differential Geometry*, 26:349–360, 1987.

[34] B. Springborn. A variational principle for weighted Delaunay triangulation and hyperideal polyhedra. *Journal of Differential Geometry*, 78(2):333–367, 2008.

[35] B. Springborn, P. Schröder, and U. Pinkall. Conformal equivalence of triangle meshes. *ACM Trans. Graph.*, 27(3):1–11, 2008.

[36] K. Stephenson. *Introduction to Circle Packing: The Theory of Discrete Analytic Functions*. Cambridge University Press, 2005.

[37] W. P. Thurston. *The Geometry and Topology of 3-manifolds*. Princeton University Press, 1981.

[38] Y. Wang, M. Gupta, S. Zhang, S. Wang, X. Gu, D. Samaras, and P. Huang. High resolution tracking of non-rigid motion of densely sampled 3d data using harmonic maps. *International Journal of Computer Vision*, 76(3):283–300, 2008.

[39] W. Brägger. Kreispackungen und triangulierugen. *Enseign. Math.*, 38:201–217, 1992.

[40] Z.-X. He. Rigidity of infinite disk patterns. *Ann. of Math*, 149(1):1–33, 1999.

[41] W. Zeng and X. Gu. *Ricci Flow for Shape Analysis and Surface Registration*. SpringerBriefs in Mathematics. Springer, New York, 2013.

[42] W. Zeng, J. Marino, K. Gurijala, X. Gu, and A. Kaufman. Supine and prone colon registration using quasi-conformal mapping. *IEEE Transactions on Visualization and Computer Graphics)*, 16(6):1348–1357, 2010.

[43] W. Zeng, D. Samaras, and X. D. Gu. Ricci flow for 3D shape analysis. *IEEE Transactions on Pattern Analysis and Machine Intelligence*, 32(4):662–677, 2010.

[44] M. Zhang, R. Guo, W. Zeng, F. Luo, S.-T. Yau and X. Gu. The unified discrete surface Ricci flow. *Graphical Models*, 76(5):321–339, 2014.

Wei Chen
School of Software and Technology
Dalian University of Technology
China
E-mail address: wei.chen@mail.dlut.edu.cn

Min Zhang
Center of Mathematical Science and Application
Harvard University
Brigham and Women's Hospital
Harvard Medical school
USA
E-mail address: mzhang@bwh.harvard.edu

Na Lei
DUT-RU International School of Information Science & Engineering
Dalian University of Technology
Key Laboratory for Ubiquitous Network and
Service Software of Liaoning Province
China
E-mail address: nalei@dlut.edu.cn

David Xianfeng Gu
Computer Science Department
Stony Brook University
USA
E-mail address: gu@cs.stonybrook.edu

Received 3 January 2017